Appendix A

Derivation of equations

A.1 Equation 3.2

Correction factor for horizontal strain at the centre of a pack measurement with LVDT's fixed at half of the original pack height

Consider the parabola in Figure A.1.

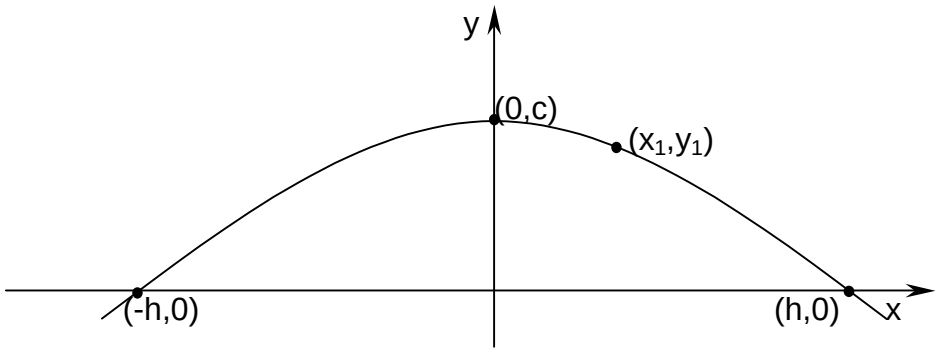

Figure A.1 Definition sketch of the parabola for the derivation of the correction factor for the fixed LVDT measurement of the horizontal deformation of the centre of the pack.

For the parabola shown in Figure A.1 it can be shown that:

$$c = \frac{h^2 \cdot y_1}{h^2 - x_1^2} = \frac{y_1}{1 - \left(\frac{x_1}{h}\right)^2} \qquad \text{(A.1)}$$

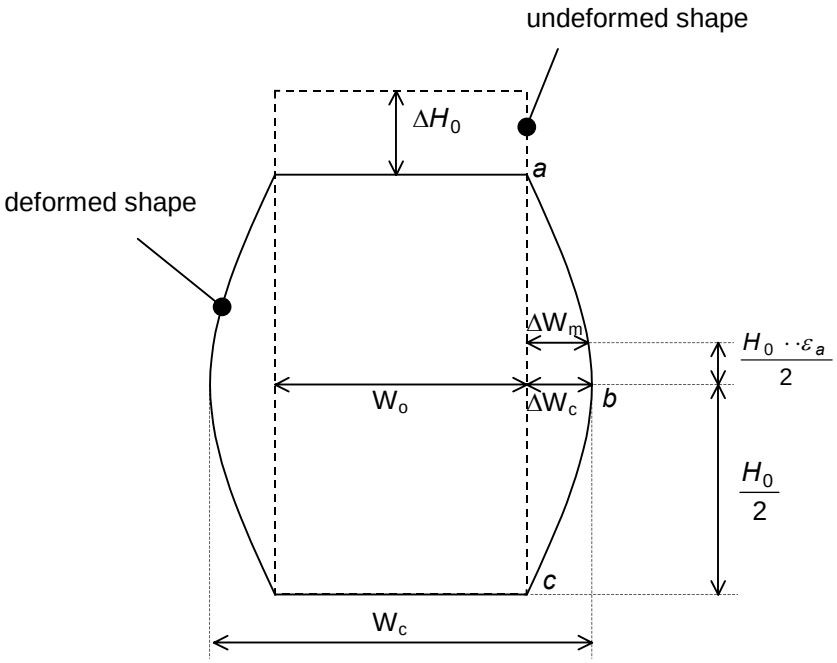

Figure A.2 Definition sketch of deformed pack for the derivation of the correction factor for the fixed LVDT measurement of the horizontal deformation of the centre of the pack.

Considering a deformed pack showed in the definition sketch in Figure A.2 and assuming the profile *a-b-c* for a pack to be a parabola, it can in similar vein be shown that:

$$\Delta W_c = \frac{\Delta W_m}{1-\left(\frac{x_1}{h}\right)^2} \tag{A.2}$$

Where:

ΔW_c = the horizontal deformation at the centre of the pack,

ΔW_m = the measured horizontal deformation at $\frac{H_0}{2}$,

x_1 = $\frac{H_0 \cdot \varepsilon_a}{2}$,

h = $\frac{H_0(1-\varepsilon_a)}{2}$.

Substitution and simplification leads to:

$$f = \frac{\Delta W_c}{\Delta W_m} = \frac{1}{1-\left(\frac{\varepsilon_a}{1-\varepsilon_a}\right)^2} \tag{A.3}$$

A.2 Equation 4.53

The depth of the "dead zone"

Consider the parabola in Figure A.3.

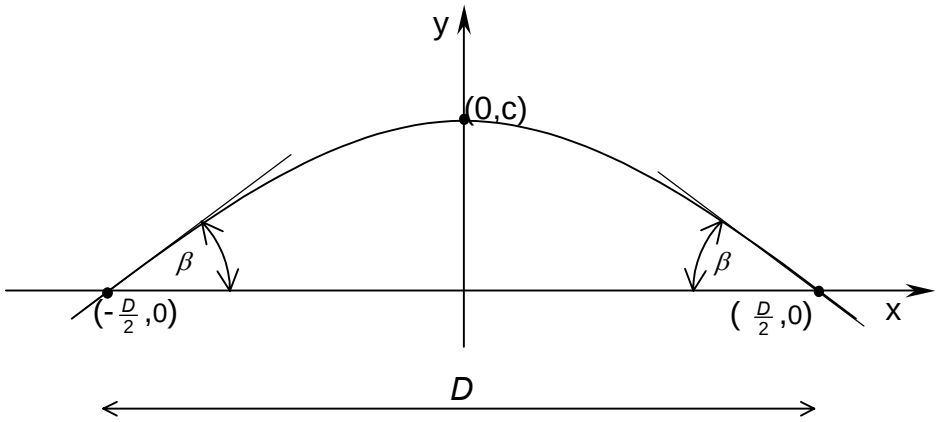

Figure A.3 Definition sketch of parabola for the derivation of the depth of the "dead zone".

The parabola shown in the definition sketch (Figure A.3) can be written as:

$$y = -\frac{c}{\left(D/2\right)^2} \cdot x^2 + c\,, \tag{A.4}$$

for which the derivative to x is:

$$\frac{dy}{dx} = -2 \cdot \frac{c}{\left(D/2\right)^2} \cdot x \tag{A.5}$$

Evaluating the derivative at $x = \frac{D}{2}$ and equalling to the tangent of the β-angle gives:

$$\left.\frac{dy}{dx}\right|_{\frac{D}{2}} = -2 \cdot \frac{c}{\left(D/2\right)} = -\tan(\beta) \tag{A.6}$$

resulting in,

$$c = \frac{D \cdot \tan(\beta)}{4} \tag{A.7}$$

A.3 Equation 4.55

The relationship between the mean axial strain in and the overall strain of a cylinder of soil

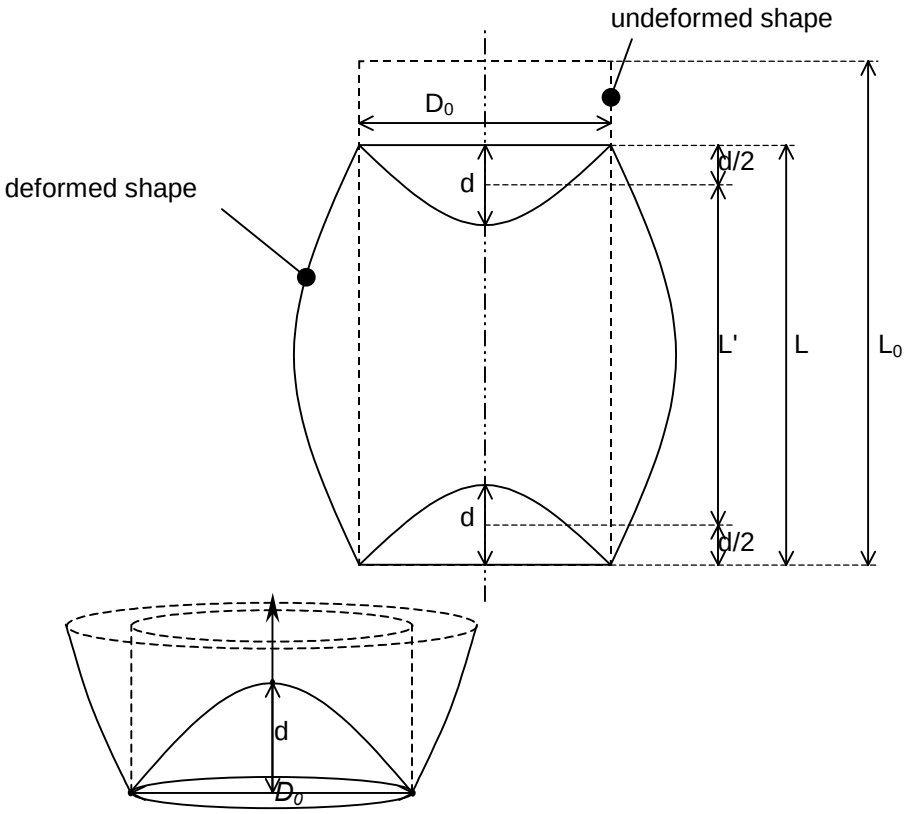

Figure A.4 Definition sketch for the derivation of the "mean" height and volume of the deformed soil cylinder.

Define ε_{ag} as the axial strain of the whole cylinder and $\bar{\varepsilon}_{al}$ as the mean local axial strain of the soil in the cylinder:

$$\varepsilon_{ag} = \frac{\Delta L}{L} \quad \text{and} \quad \bar{\varepsilon}_{al} = \frac{\Delta L}{L'} \tag{A.8}$$

Where:

ε_{ag} = the axial strain of the whole cylinder,

$\bar{\varepsilon}_{al}$ = the mean local axial strain of the soil in the cylinder,

L = the length of the deformed cylinder,

L' = the mean length of the soil cylinder outside of the "dead zone".

Consider the definition sketch of a deformed cylinder shown in Figure A.4.

The volume of the paraboloid shown in Figure A.4 is:

$$V_p = \frac{\pi \cdot {D_0}^2}{4} \cdot \frac{d}{2} \tag{A.9}$$

Where:

V_p = the volume of the paraboloid,

d = the height of the paraboloid,

D_0 = the diameter of the base of the paraboloid.

The "mean" height of the "dead zone" is therefore $\frac{d}{2}$ and the mean length of the soil cylinder outside of the "dead zone" is given by:

$$L' = L - d \tag{A.10}$$

which, by virtue of Equation (A.7), can be written as:

$$L' = L - \frac{D_0}{4} \cdot \tan(\beta) \tag{A.11}$$

Where:

β = the angle between the boundary of the "dead zone" and the end of the cylinder.

The length of the deformed cylinder can be written as:

$$L = L_0 \cdot (1 - \varepsilon_{ag}) \tag{A.12}$$

Substitution of Equation (A.8) and (A.12) into (A.11) results in the following relationship between the overall and mean local axial strain:

$$\varepsilon_{ag} = \bar{\varepsilon}_{al} \cdot \left(1 - \frac{D_0}{L_0 \cdot (1 - \varepsilon_{ag}) \cdot 4} \cdot \tan(\beta)\right) \tag{A.13}$$

A.4 Equation 4.56

The relationship between the mean volumetric strain in and the overall volumetric strain of a cylinder of soil

Define ε_{vg} as the axial strain of the whole cylinder and $\bar{\varepsilon}_{vl}$ as the mean local axial strain of the soil in the cylinder, that is:

$$\varepsilon_{vg} = \frac{\Delta V}{V} \quad \text{and} \quad \bar{\varepsilon}_{vl} = \frac{\Delta V}{V'} \tag{A.14}$$

Where:

ε_{vg} = the volumetric strain of the whole soil cylinder,

$\bar{\varepsilon}_{vl}$ = the mean local volumetric strain of the soil in the cylinder,

V = the volume of the deformed cylinder,

V' = the mean volume of the soil outside of the "dead zone".

$$V_p = \frac{\pi \cdot D_0^{\,2}}{4} \cdot \frac{d}{2} \tag{A.15}$$

Where:

V_p = the volume of the paraboloid,

d = the height of the paraboloid,

D_0 = the diameter of the base of the paraboloid.

The "mean" volume of the soil outside of the "dead zone" is given by:

$$V' = V - 2 \cdot V_p = V - V_p = \frac{\pi \cdot D_0^{\,2}}{4} \cdot \frac{D_0}{4} \cdot \tan(\beta) \tag{A.16}$$

This equation can be written as:

$$V' = V - \frac{V_0}{L_0} \cdot \frac{D_0}{4} \cdot \tan(\beta) = V\left(1 - \frac{D_0}{L_0 \cdot (1-\varepsilon_{vg}) \cdot 4} \cdot \tan(\beta)\right) \tag{A.17}$$

Substitution of Equation (A.14) into Equation (A.17) results in the following relationship between the overall and mean local volumetric strain:

$$\varepsilon_{vg} = \bar{\varepsilon}_{vl} \cdot \left(1 - \frac{D_0}{L_0 \cdot (1-\varepsilon_{vg}) \cdot 4} \cdot \tan(\beta)\right) \tag{A.18}$$

A.5 Equation 4.58

The radius at the centre of the deformed cylinder in terms of its original dimensions and the axial and volumetric strain – high ambient confining stress

Consider the definition sketch of a deformed cylinder shown in Figure A.5.

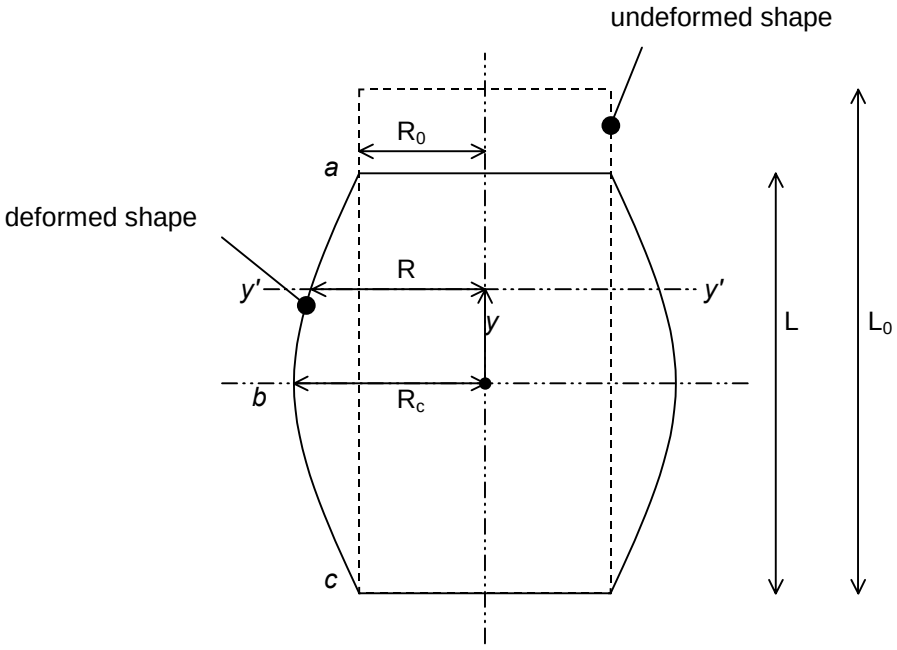

Figure A.5 Definition sketch of the deformed cylinder under conditions of high ambient confining stress.

Assuming the deformation profile of *a-b-c* to be parabolic it can be shown that:

$$R = \frac{4 \cdot (R_0 - R_c)}{L^2} \cdot y^2 + R_c \qquad \text{(A.19)}$$

Where:

R = the radius of the deformed cylinder at section *y'-y'*,
R_0 = the original radius of the cylinder,
R_c = the radius at the centre of the deformed cylinder,
L = the length of the cylinder.

The cross sectional area of the deformed cylinder at *y'-y'* can be written as:

$$A = \pi \cdot R^2(y) \qquad \text{(A.20)}$$

Where:

A = the cross sectional area of the deformed cylinder at section *y'-y.'*

The volume of the deformed cylinder can be obtained by integrating the area over the height of the deformed cylinder:

$$V = \int_{-\frac{L}{2}}^{\frac{L}{2}} A \cdot dy = \int_{-\frac{L}{2}}^{\frac{L}{2}} \pi \cdot R^2(y) \cdot dy \tag{A.21}$$

Evaluating Equation (A.21) leads to the following expression for the volume:

$$V = \frac{\pi}{15} \cdot L \cdot \left(3 \cdot {R_0}^2 + 4 \cdot R_0 \cdot R_c + 8 \cdot {R_c}^2\right) \tag{A.22}$$

Where:

V = the volume of the deformed cylinder.

Solving for R_c results in the following expression:

$$R_c = \sqrt{\frac{5}{16} \cdot \left(\frac{6}{\pi} \cdot \frac{V}{L} - {R_0}^2\right)} - \frac{R_0}{4} \tag{A.23}$$

The volume and the length of the deformed cylinder can be written in terms of its original undeformed values, as follows:

$$V = V_0 \cdot (1 - \varepsilon_v) \quad \text{and,} \tag{A.24}$$

$$L = L_0 \cdot (1 - \varepsilon_a) \tag{A.25}$$

Where:

ε_v and ε_a = the volumetric and axial strain of the cylinder respectively.

Substitution of Equation (A.24) and Equation (A.25) into Equation (A.23) leads to the following expression for the radius at the centre of the deformed cylinder in terms of its original dimensions and the axial and volumetric strain under conditions where the ambient confining stress is high compared to the confining stress caused by the membrane:

$$R_c = \sqrt{\frac{5}{16} \cdot \left(\frac{6}{\pi} \cdot \frac{V_0 \cdot (1 - \varepsilon_v)}{L_0 \cdot (1 - \varepsilon_a)} - {R_0}^2\right)} - \frac{R_0}{4} \tag{A.26}$$

A.6 Equation 4.59

The radius at the centre of the deformed cylinder in terms of its original dimensions and the axial and volumetric strain – low ambient confining stress

Consider the definition sketch of a deformed cylinder shown in Figure A.6.

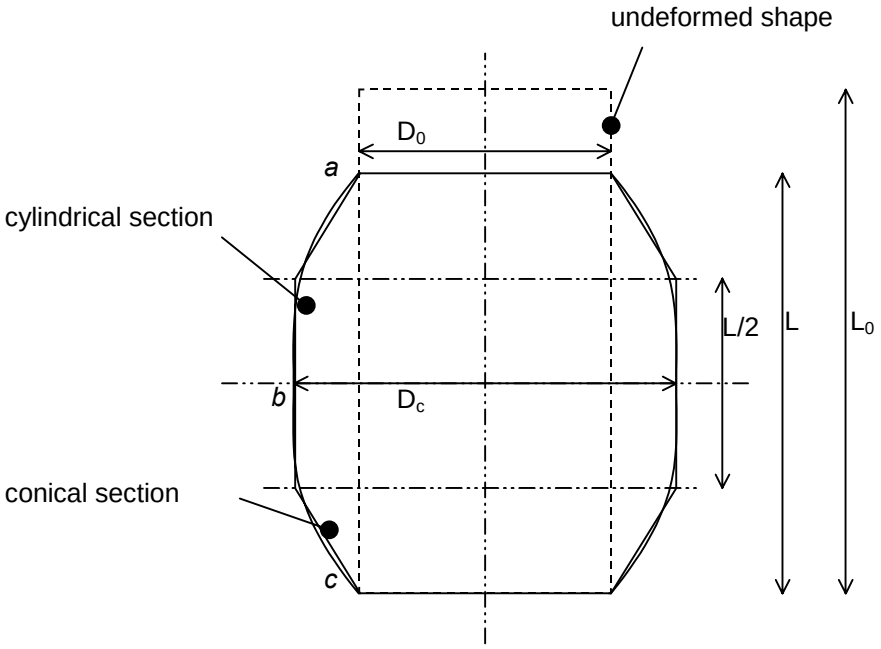

Figure A.6 Definition sketch of the deformed cylinder under conditions of low ambient confining stress.

Approximate the shape of the deformed cylinder as a cylindrical section and two conical sections as shown in Figure A.6. The volume of the deformed cylinder can then be approximated as:

$$V = 2 \cdot \frac{\pi}{4} \cdot \frac{1}{3} \cdot \left(D_0{}^2 + D_0 \cdot D_c + D_c{}^2 \right) \cdot \frac{L}{4} + \frac{\pi}{4} \cdot D_c{}^2 \cdot \frac{L}{2} \qquad \text{(A.27)}$$

Where:

D_0 = the original diameter of the cylinder,

D_c = the diameter at the centre of the deformed cylinder,

L = the length of the cylinder.

Solving for D_c results in the following expression:

$$D_c = \frac{1}{8} \cdot \left(\sqrt{\frac{384}{\pi} \cdot \frac{V}{L} - 15 \cdot D_0} - D_0 \right) \tag{A.28}$$

Substitution of Equation (A.24) and Equation (A.25) into Equation (A.28) leads to the following expression for the diameter at the centre of the deformed cylinder in terms of its original dimensions and the axial and volumetric strain under conditions where the ambient confining stress is low compared to the confining stress caused by the membrane:

$$D_c = \frac{1}{8} \cdot \left(\sqrt{\frac{384}{\pi} \cdot \frac{V_0 \cdot (1 - \varepsilon_v)}{L_0 \cdot (1 - \varepsilon_a)} - 15 \cdot D_0} - D_0 \right) \tag{A.29}$$

A.7 Equation 4.61

The confining stress imposed onto a cylinder of soil by a membrane

Consider a membrane encased soil cylinder as shown in Figure A.7.

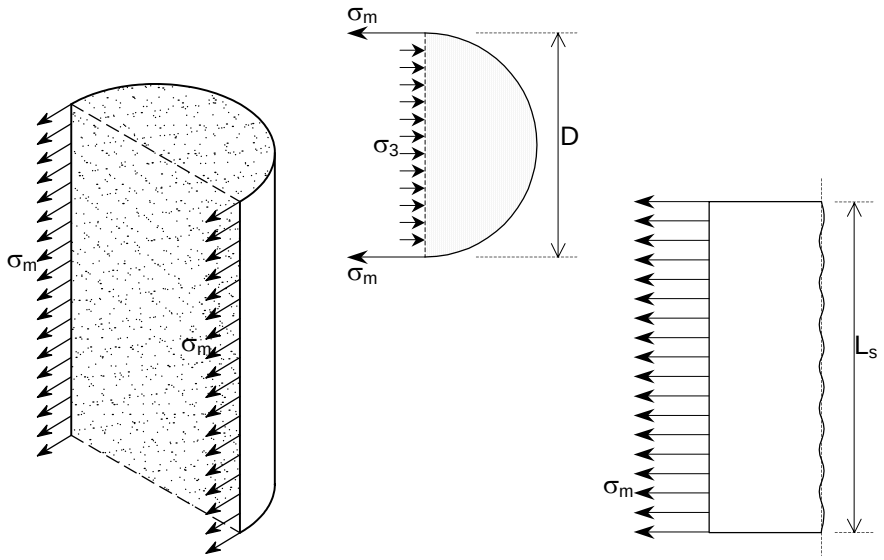

Figure A.7 Section through a soil cylinder encased in a geocell.

The force, F in the membrane per length, L_p, of the cylinder membrane can be written as:

$$F = t \cdot L_p \cdot \sigma_m \tag{A.30}$$

Where:

t = the thickness of the membrane,

L_p = the length of the membrane,

σ_m = the membrane stress.

Assuming horizontal equilibrium, the following equation can be written:

$$2 \cdot F = 2 \cdot t \cdot L_p \cdot \sigma_m = \sigma_3 \cdot D \cdot L_s \tag{A.31}$$

Where:

F = the force in the membrane,

D = the diameter of the cylinder,

L_s = the length of the soil cylinder.

Reorganizing Equation (A.31) leads to the following equation:

$$\sigma_3 = \frac{2 \cdot t}{D} \cdot \sigma_m \cdot \frac{L_p}{L_s} \tag{A.32}$$

Due to buckling of the membrane L_p is not equal to L_s. An estimate of the ratio $\frac{L_p}{L_s}$ can be obtained by writing the length of the membrane and the soil cylinder in terms of axial strain of the soil and the circumferential strain in the membrane:

$$\frac{L_p}{L_s} = \frac{1 - \varepsilon_m \cdot \nu_m}{1 - \varepsilon_a} \tag{A.33}$$

Where:

ε_m = the circumferential strain in the membrane,

ν_m = the Poisson's ratio of the membrane,

ε_a = the axial strain of the soil.

A.8 Equation 4.62

The mean radius of the centre half of a deformed soil cylinder

Refer to the definition sketch shown in Figure A.5. The parabolic profile of the deformed cylinder can be written as (Cf. Equation (A.19)):

$$R = \frac{4 \cdot (R_0 - R_c)}{L^2} \cdot y^2 + R_c \qquad \text{(A.19)}$$

The mean radius over the centre half of the deformed cylinder can be obtained by integrating Equation (A.19) from $y = 0$ to $y = L/4$ and dividing by L/4:

$$\overline{R} = \frac{\int_0^{\frac{L}{4}} R(y)dy}{\frac{L}{4}} = \frac{4}{48} \cdot (R_0 + 11 \cdot R_c) \qquad \text{(A.34)}$$

Where:

$\overline{R}$ = the mean radius of the centre half of the deformed cylinder,

R_0 = the original radius of the cylinder,

R_c = the radius at the centre of the deformed cylinder,

L = the length of the cylinder.

Appendix B

Relationships between the limiting friction angles

B.1 Introduction

The values of the limiting friction angle for a clean sand ϕ'_{μ} (the interparticle friction angle), and ϕ'_{cv} (the friction angle at constant volume shearing), are important for the quantification of the stress-dilatancy behaviour of the sand. Due to the difficulties in obtaining these values, a relationship between these values will have great practical value. Several relationships between the limiting angles have been presented in the past.

B.2 The relationship between the limiting friction angles

Caquot (1934) derived the following expression for plane strain conditions:

$$\phi'_{cv} = \operatorname{atan}\left(\frac{\pi}{2}\cdot\tan\left(\phi'_{\mu}\right)\right) \tag{B.1}$$

Bishop (1954) presented the following equations:

$$\phi'_{cv} = \operatorname{asin}\left(\frac{3}{2}\cdot\tan\left(\phi'_{\mu}\right)\right) \quad \text{for plane strain and} \tag{B.2}$$

$$\phi'_{cv} = \operatorname{asin}\left(\frac{15\cdot\tan\left(\phi'_{\mu}\right)}{10+3\cdot\tan\left(\phi'_{\mu}\right)}\right) \quad \text{for triaxial compression.} \tag{B.3}$$

Horn (1969) presented the relationship shown with the others in Figure B.1. This relationship is not presented in a closed form and involves the simultaneous solution of the following equations:

$$\beta_1 = \frac{\pi}{2} - \phi'_\mu$$
$$2\beta_1 + \sin(2\beta_1) + 2\cdot\cos(2\beta_1) = 2\beta_2 + \sin(2\beta_2) + 2\cdot\cos(2\beta_2) \quad \text{(B.4)}$$

Which can, with

$$\frac{\sigma'_1}{\sigma'_1 - \sigma'_3} = \frac{1}{3}\cot(\phi'_\mu)\cdot\left(\frac{\cos^3(\beta_2) - \cos^3(\beta_1)}{\sin(\beta_1) - \sin(\beta_2)}\right) + 1 - \frac{1}{3}\cdot\left(\sin^2(\beta_1) + \sin(\beta_1)\sin(\beta_2) + \sin^2(\beta_2)\right) \quad \text{(B.5)}$$

and

$$\frac{\sigma'_1}{\sigma'_3} = \tan^2\left(\frac{\pi}{4} + \frac{\phi'_{cv}}{2}\right) \quad \text{(B.6)}$$

be used to obtain the value of ϕ'_{cv} from ϕ'_μ.

The author suggest that the relationship presented by Horn could be approximated by the following polynomial function:

$$\phi'_{cv} = 0.00036\phi'^{\,3}_\mu - 0.036\phi'^{\,2}_\mu + 1.965\phi'_\mu \quad \text{(B.7)}$$

Skinner (1969), however, presented data in complete disagreement with these theoretical curves and points out that in the derivation of the theoretical relationships, particle rolling as a permissible mechanism is excluded. Skinner stated that there is no direct relationship between ϕ'_{cv} and ϕ'_μ, a sentiment shared by Green (1971) and Bishop (1971). Bishop (1971) pointed out that he could not fault Skinner's work on the basis either of technique or of interpretation. Rowe (1971b) regarded Skinner's work with scepticism and stated that the data was insufficient to support the mentioned claim and that the reason for Skinner's observations needed further investigation.

Skinner's claim that no relationship exist between the two limiting angles is contradicted by the results of Thornton (2000) who performed 3D Discrete Element Modelling[1] on a polydisperse system of elastic spheres subject to axisymmetric compression. He pointed out that a random assembly of frictionless spherical particles are unstable at all interparticle contacts, which prevents a force transition through the system. A low ϕ'_μ will therefore lead to a low ϕ'_{cv}, as suggested by Horn (1969). The results of Thornton (2000),

[1] Thornton used the software "TRUBALL" developed by Peter Cundall (1988) which is the predecessor of the software PFC 3D. (More information is available at http://www.hcitasca.com/)

however, deviates significantly from the relationship presented by Horn and for ϕ'_μ >25° is closer to the data presented by Skinner (1969) than to Horn's theoretical relationship. Thornton suggests that the difference between the numerical results and Horn's theory arises from the fact that the theory ignores the possibility of particle rotation. Thornton states that when particle rotation was prevented in the analyses the shear strength was significantly increased. He believes that the data from the analyses may approach Horne's theoretical relationship if rotation is completely inhibited.

Data of the value of the two limiting angles presented in literature is tabulated in Table B.1 and plotted in Figure B.1 with the theoretical relationships presented earlier. It can be seen that, ignoring the data presented by Skinner, there seems to exist a strong relationship between the two limiting angles.

Horn's theoretical relationship seems to slightly overestimate the value of ϕ'_{cv} for a given value of ϕ'_μ. The following relationship provides a slightly better fit to the data:

$$\phi'_{cv} = 0.0001373\phi'^{3}_{\mu} - 0.019\phi'^{2}_{\mu} + 1.67\phi'_{\mu} \qquad \text{(B.8)}$$

A possible explanation of the discrepancy between the work of Skinner and the other researchers is that Skinner aimed to measure the true inter-particle friction, while the other researchers were more interested in obtaining the parameter, ϕ'_μ, applicable to Rowe's theory. It is quite possible that the parameter ϕ'_μ, in Rowe's theory, might not be the true inter-particle friction angle but rather, a manifestation of the true friction angle and other variables associated with the microscopic inter-particle mechanical behaviour of the granular assembly.

It is interesting to note that both Skinner's (1969) tests and Thornton's (2000) analyses were performed on assemblies of perfectly spherical particles. Due to the higher degree of dilation that would be associated with the rotation of non-spherical particles compared to interparticle sliding, one would expect therefore that sliding, rather than rolling of the particles would be favoured in assemblies of non-spherical particles, which may be a contributing factor to the discrepancy between the data presented by Skinner (1969) and the other researchers.

Table B.1 Data of the two limiting angles presented in literature.

ϕ'_{μ} (°)	ϕ'_{cv} (°)	Material type	Reference
27.35	32.6	Ham River sand	Bishop & Green (1965)
38	42	Quartz sand	Bromwell (1966)
28	36	Quartz sand	Bromwell (1966)
27	33	Brasted River sand	Cornforth (1964)
37.6	41.5	Limestone sand	Billam (1971)
35	46	Granulated chalk	Billam (1971)
31.2	36.8	Crushed anthracite	Billam (1971)
29	34	Karlsruhe sand	Hettler & Vardoulakis (1984)
28.5	34	Quartz sand, well graded, angular	Hanna (2001)
27	33.5	Quartz sand, uniform, angular particles	Hanna (2001)
24.8	32	Quartz sand, uniform, rounded particles	Hanna (2001)
24	33.3	Sacramento river sand	Lee & Seed (1967)
24	30	Ottawa sand	Lee & Seed (1967)
36	41	Feldspar	Lee (1966)
39	43	Crushed glass	Parikh (1967)
28	35	Quartz sand	Parikh (1967)
20	27	Bronze spheres	Parikh (1967)
26	32	Mersey river quartz sand	Rowe (1962)
17	24	Glass ballotini	Rowe (1962)
27	32	Quartz sand	Rowe (1965)
23	29	Zircon	Rowe (1969)
29	34.4	Hostun sand	Schanz & Vermeer (1996)
29	34.375	Cycloned gold tailings (Quartzitic silty fine sand)	
9	13.8-17	Steel	Horn (1969)
1.7 - 5.1	22 - 28	Glass ballotini - dry (1mm)	Skinner (1969)
26.6 - 38.7	19 - 29	Glass ballotini - flooded (1mm)	Skinner (1969)
1.7 - 6.8	22 - 26	Glass ballotini - dry (3mm)	Skinner (1969)
38.3 - 41.7	23 - 29	Glass ballotini - flooded (3mm)	Skinner (1969)
16.2 - 33.4	17 - 27	Steel - dry (3.175mm)	Skinner (1969)
4 - 6.8	22 - 28	Lead shot - dry (3mm)	Skinner (1969)

This, however, has more academic than practical value and from a pragmatic point of view can be ignored. It is therefore suggested that within the framework of the stress-dilatancy theory, the previously mentioned relationship between ϕ'_{μ} and ϕ'_{cv} can be assumed.

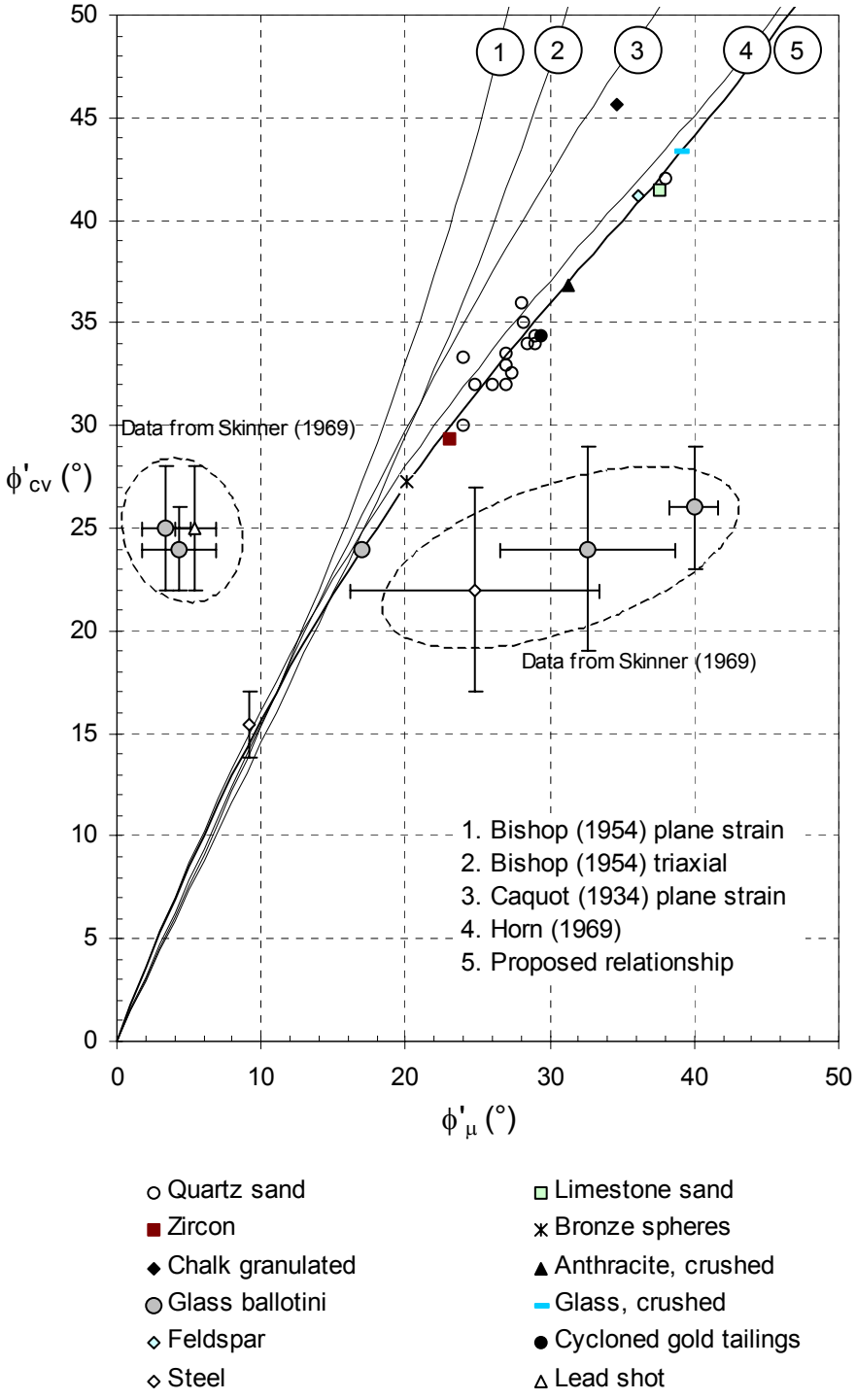

Figure B.1 The relationship between the two limiting angles.

Appendix C

Formulation of a constitutive model for the fill material

C.1 Introduction

This section of the thesis aims at extending the stress-dilatancy theory discussed in Section 4.4 into a constitutive model. Numerous constitutive models have been presented over the last couple of decades, which raises the question whether the need exists for another constitutive model, and what could be achieved by such a venture? It, therefore, seems appropriate to first put this work into the proper perspective, before continuing.

Soil can be described as a non-linear, inelastic, anisotropic and non-homogenous material with stress, stress path and time dependent behaviour. It is due to this complex behaviour of soil that the numerous constitutive models exist.

Yong and Selig (1980), however, were of the opinion that none of the models available in 1980, when the ASCE Symposium on Limit Equilibrium, Plasticity and Generalized Stress-Strain Applications in Geotechnical Engineering was held, was able to completely represent the complex behaviour of soil. A sentiment echoed by Christian (1980) who also states that there is inevitably some error in any model and that each model works best in an application for which it was developed and may not work at all in another application. It is therefore important to determine which characteristics of the soil are relevant to the particular engineering problem, and try to model only those aspects of the behaviour (Christian, 1980; Baladi, 1980). Baladi (1980) also warns against applying a specific constitutive model beyond its range of applicability.

Many of the constitutive models presented during the last couple of decades introduce new formulations of yield criteria, flow rules and hardening relationships, which necessitates several new parameters that cannot easily be obtained from commercially available laboratory tests.

From a practical point of view, Baladi (1980) suggests that the number of parameters should be kept to a minimum and the numerical values of these parameter should be readily derivable from laboratory test data. He also states that the parameters should not merely be a set of numbers generated through a trial-and-error "black box" routine to fit a given set of data, but that they have physical significance in terms of compressibility, shear strength, etc., so that when extrapolating to different materials, rational engineering judgements can be made as to their relative magnitudes based on geologic descriptions, mechanical properties and other conventional indices (Baladi, 1980).

This is achievable by using the stress-dilatancy theory as a basis for the constitutive model.

It is Duncan's (1980) experience that more than half of the time and effort involved in typical stress-strain applications in geotechnical engineering is devoted to considering the uncertainties that is invariably part of any geotechnical project. To him, it seems more appropriate to employ fairly simple stress-strain relationships, as a high degree of precision in matching field behaviour is unlikely, even with the most sophisticated relationship.

Yong and Selig (1980) states that:

> *"some constitutive models are too complex or too difficult to use in solving geotechnical problems".*

A sentiment shared by Chan (1998) when he states that comprehensive models are difficult to understand. It, therefore, is desirable to make use of models, which are just sufficiently complex for the intended application in order to minimize the burden of determination of soil parameters (Muir Wood, 1998).

Chan (1998) end his discussion on the use of comprehensive soil models in geotechnical analysis with a reference to the following quotation which has been attributed to Albert Einstein:

> *"As simple as possible, but no simpler".*

In light of these comments and suggestions it is desirable to use the simplest possible constitutive model, for which the necessary parameters can be obtained from standard laboratory tests and takes into account the characteristics of the soil behaviour, most relevant to the particular problem it is being applied to.

The simple and robust constitutive models provided as standard options in commercially available geotechnical numerical analysis software are normally, the Elasto-plastic Mohr-Coulomb model (Shield, 1955), the Duncan-Chang model (Duncan and Chang, 1970) and the Cam-clay or Modified Cam-clay models (Roscoe et al., 1958; 1963). None of these models, however, takes the work hardening and the non-associated flow of the material into account. The stress-dilatancy behaviour of the soil is, therefore, not accounted for in these models.

Most of the commercially available software have incorporated non-associated flow into the Mohr-Coulomb models and some, like the finite difference codes FLAC and FLAC3D, provides a model with user specified hardening/softening behaviour for both the strength and dilational parameters. Such models form platforms with which the constitutive model presented in this section can be incorporated into numerical analyses.

C.2 The constitutive model

In its simplest form, elasto-plastic constitutive models consist of elastic material behaviour, a yield criterion and a flow rule. The yield criterion defines the stress state at which the material start deforming plastically while the flow rule defines a relationship between the yield surface and the plastic strain increment vector used to calculate the plastic strain component.

For failure problems, the use of elasto-plastic Mohr-Coulomb material models will often suffice. Such models are, however, not suitable for studying the behaviour of the soil under working loads, conditions with large variations in σ'_3, or under conditions of large strains, as it overestimates the elastic range.

For these conditions, a work-hardening/softening model will be necessary. The cycloned tailings material, and sands in general, exhibit a work-hardening plastic behaviour up to a peak strength after which strain softening occurs. The difference between elastic-perfectly plastic models and isotropic work-hardening models are shown in Figure C.1.

The elastic behaviour, yield criterion, flow rule and hardening law will be discussed in the following paragraphs.

C.2.1 The elastic range

The elastic component of the material model was discussed in Section (4.3.1). The stiffness referred to, is applicable to higher intermediate and large strains. The presented model is not applicable to the small strain ranges and therefore suffers the same limitations as the most common constitutive models (e.g. the Cam-clay model and the Hyperbolic model presented by Duncan and Chang (1970) (Lo Presti et al., 1998)).

C.2.2 The yield surface

Over the years, many researchers have advanced the knowledge of the yield surface applicable to sand or other granular material. Amongst others, such advances have been made by Green and Bishop (1969), Shibata and Karube (1965), Preace (1971), Matsuoka and Nakai (1982), Goldscheider (1984). The work of the mentioned researchers are shown in Figure C.2 as measured data plotted on the deviatoric stress plane, along with the applicable Mohr-Coulomb yield surface. Vermeer and de Borst (1984) suggest that, for most engineering purposes, the deviation from the Mohr-Coulomb surface is not large enough to warrant the use of another more complicated surface. For this reason, a yield surface of the Mohr-Coulomb type is assumed. The yield surface can therefore be formulated as:

$$R = \frac{\sigma'_1}{\sigma'_3} = \frac{1+\sin(\phi'_{mob})}{1-\sin(\phi'_{mob})} \qquad \text{(C.1)}$$

Where:

ϕ'_{mob} = the mobilized internal angle of friction.

From Rowe's stress-dilatancy theory, the following relationships relating the Mohr-Coulomb friction angle, ϕ'_f, to the dilation angle, ψ, and the Rowe friction angle can be obtained:

$$\sin(\phi'_{mob}) = \frac{\sin(\phi'_f)+\sin(\psi)}{1+\sin(\phi'_f)\cdot\sin(\psi)} \qquad \text{(C.2)}$$

Where:

ϕ'_{mob} = the mobilized internal angel of friction,

ϕ'_f = the Rowe friction angle,

ψ = the dilation angle.

Rowe's stress-dilatancy theory can therefore easily be implemented into numerical analysis software by assuming a Mohr-Coulomb material for which the Mohr-Coulomb friction angle is given by the relationship in Equation (C.2).

C.2.3 The hardening behaviour and flow rule

In the hardening model the elastic range is a function of the plastic strain. The simplest form of work-hardening models is isotropic hardening, which assumes that the centre of the yield surface does not change during loading, that is, the yield surface in σ'_1 - σ'_2 - σ'_3 space remains symmetrical around the space diagonal $\sigma'_1 = \sigma'_2 = \sigma'_3$. Test data normally available to practicing engineers does not warrant the use of a more complicated assumption.

In order to quantify the hardening behaviour of the material, a parameter called the hardening parameter, needs to be specified which are a measure of the plastic strain in the material.

Vermeer and De Borst (1984) state that for granular material the effective plastic shear strain is suitable for use as a hardening parameter. In this regard they refer to the work of Stroud (1971) and Tatsuoka and Ishihara (1975) who report evidence for quantities that resemble the effective strain very closely.

The hardening parameter employed by Vermeer (1978) can be written as:

$$\kappa_p = \frac{1}{\sqrt{2}} \cdot \sqrt{\left(\varepsilon_1^p - \varepsilon_2^p\right)^2 + \left(\varepsilon_2^p - \varepsilon_3^p\right)^2 + \left(\varepsilon_3^p - \varepsilon_1^p\right)^2} = \frac{3}{2} \cdot \varepsilon_s^p \qquad \text{(C.3)}$$

Where:

κ_p = the hardening parameter used by Vermeer (1978),

ε_1^p, ε_2^p, ε_3^p = the plastic components of the major, intermediate and minor principal strain,

ε_s^p = the plastic shear strain.

The plastic shear strain, ε_s^p, will be used as the hardening parameter in this document and has proven adequate for the tested material.

A common approach for modelling the work-hardening/softening behaviour of soil is to apply a hardening function to the Mohr-Coulomb friction angle, which

results in an increase (decrease in the case of softening) in the size of the yield surface with an increased plastic shear strain. This is also the approach suggested by Vermeer and De Borst (1984).

Rowe's stress-dilatancy theory, however, provides some insight into the mechanism by which the work-hardening in the granular material takes place. According to the theory, the increase in the size of the Mohr-Coulomb yield surface with plastic shear strain is mainly due to an increase in the dilational behaviour of the material with an increase in the plastic shear strain. Similarly, work softening takes place as a result of a decrease in the dilational behaviour of the material.

The approach presented here is to apply a work-hardening/softening function to the dilational behaviour of the material and with the use of Rowe's stress-dilatancy theory (using Equation (C.2)), obtain the strength of the material. Equation (C.2) therefore provides the flow rule for the model.

This approach is equivalent to applying Rowe's stress-dilatancy theory as a flow rule. The normal use of the flow rule is to calculate the plastic shear strain increment from the yield surface. The suggested approach, however, uses the flow rule to calculate the yield surface from the plastic shear strain increment.

Using Rowe's stress-dilatancy theory as a flow rule implicitly assumes non-associated flow according to the stress-dilatancy theory. Normality is, however, assumed in the deviatoric stress plane. The plastic potential therefore will have the same shape as the Mohr-Coulomb yield surface in the deviatoric stress plane, that is, the plastic potential function, *g*, is given by:

$$g = \sigma_1' + \sigma_3' \cdot \left(\frac{1 + \sin(\psi)}{1 - \sin(\psi)} \right) \tag{C.4}$$

An assumption proven to be acceptable by Goldscheider (1984).

The use of Rowe's stress-dilatancy theory as a flow rule has been suggested by other researchers as well (Vermeer, 1978; Wan and Guo, 1998).

In order to model the work hardening behaviour of the soil a hardening function was applied to the dilational parameter, *D*. Rowe (1971a) suggested a complex function for *D* as a function of the major principal shear strain. His function is applicable over the total range of ε_s^p and needs to be fitted to the stress strain data in the pre- and post-peak range via a non-linear curve fitting technique. It was found that this equation does not provide a good fit for the pre-peak data of

the cycloned tailings. In general, practicing engineers seldom have enough good quality data in the post-peak range to justify using this approach.

Several useful work-hardening functions were presented by Brinch Hansen (1965). Vermeer and De Borst (1984) state that the following function applied as a work-hardening function to the Mohr-Coulomb friction angle yielded satisfactory results for most sands:

$$f_1 = \frac{2 \cdot \sqrt{\varepsilon_s^p \cdot \left(\varepsilon_s^p\right)_{peak}}}{\varepsilon_s^p + \left(\varepsilon_s^p\right)_{peak}} \tag{C.5}$$

Where:

f_1 = the hardening function applicable to the pre-peak plastic strain,

ε_s^p = the hardening parameter, plastic shear strain,

$(\varepsilon_s^p)_{peak}$ = the plastic shear strain at peak strength.

This hardening function proved useful when applied to D up to the shear strain at peak dilation. After the plastic shear strain at peak is reached, strain softening of the dilational parameter, D, occurs so that D approaches a value of 1, which corresponds to a dilation angle of $\psi = 0°$. When this state is reached, the material exhibits a constant volume behaviour and an internal angle of friction equal to ϕ'_{cv} is applicable.

For the post-peak softening of the dilation behaviour of the material the following empirical equation is suggested:

$$f_2 = 1 - A^2 \cdot (3 - 2 \cdot A) \tag{C.6}$$

With:

$$A = \left(\frac{\ln\left(\varepsilon_s^p\right) - \ln\left(\left(\varepsilon_s^p\right)_{peak}\right)}{\ln\left(\left(\varepsilon_s^p\right)_{cv}\right) - \ln\left(\left(\varepsilon_s^p\right)_{peak}\right)} \right)$$

Where:

f_2 = the hardening function applicable to the post-peak plastic strain,

ε_s^p = the hardening parameter, plastic shear strain,

$(\varepsilon_s^p)_{peak}$ = the plastic shear strain at peak,

$(\varepsilon_s^p)_{cv}$ = the plastic shear strain at which the dilation parameter can be assumed to be 1.

The value of $(\varepsilon_s^p)_{cv}$ governs the rate of the post-peak strain softening. For the tested cycloned tailings, the value of $(\varepsilon_s^p)_{cv}$ seems to be constant at about 0.47.

In order to complete the strain hardening function, the value of D at the start of plastic shearing needs to be estimated.

From Rowe's stress-dilatancy theory the following relationship can be derived:

$$D_0 = \frac{1+\sin(\psi_0)}{1-\sin(\psi_0)} \tag{C.7}$$

With:

$$\sin(\psi_0) = \frac{\sin(\phi'_0) - \sin(\phi'_{initial})}{1-\sin(\phi'_0)\cdot\sin(\phi'_{initial})}$$

Where:

$\phi'_{initial}$ = ϕ'_{cv} for plain strain conditions,

$\phi'_{initial}$ = ϕ'_{μ} for triaxial strain conditions,

ϕ'_0 = the internal angle of friction before the onset of work hardening.

The value of ϕ'_0 is a measure of the size of the initial Mohr-Coulomb yield surface and can be obtained from triaxial testing data with:

$$\sin(\phi'_0) = \frac{1-R_0}{1+R_0} \tag{C.8}$$

Where:

R_0 = the stress ratio at the start of plastic behaviour.

For the tested material over the range of densities and confining stresses tested, the value of R_0 was found to be approximately 1.3. A constant value of 1.3 was used, which corresponds to a D_0 = 0.446. This relates to an initial dilation angle ψ = -22.5°, which relates to plastic collapse at the initial stages of the plastic deformation. The phenomenon of an initial plastic collapse for sands has also been noted by other researchers (e.g. Rowe, 1971a; Papamichos and Vardoulakis, 1995).

The full strain hardening equation for D can be written as:

$$D = \begin{cases} (D_{\max} - D_0)\cdot f_1 + D_0 & \varepsilon_s^p \le (\varepsilon_s^p)_{peak} \\ (D_{\max} - 1)\cdot f_2 + 1 & \text{for } (\varepsilon_s^p)_{peak} < \varepsilon_s^p \le (\varepsilon_s^p)_{cv} \\ 1 & \varepsilon_s^p > (\varepsilon_s^p)_{cv} \end{cases} \tag{C.9}$$

Where:

D = Rowe's dilatancy parameter,

D_{max} = the maximum value of D,

D_0 = the initial value of D at the start of plastic deformation,

f_1 = the hardening function applicable to the pre-peak plastic strain,

f_2 = the hardening function applicable to the post-peak plastic strain.

Data presented by Rowe (1971a) for a dense sand tested at a confining stress of 70 kPa is shown in Figure C.3 fitted with the function presented in Equation (C.9). The value of $(\varepsilon_s^p)_{cv}$ in this case was 0.45. It is interesting in this regard to note that Thornton (2000) performing 3D Discrete Element modelling has found that for his analyses, the critical voids ratio was attained at an axial strain of about 50% which would correspond to a $(\varepsilon_s^p)_{cv}$ of slightly less than 0.5.

Figure C.3 indicates that the work-hardening/softening function presented here may be applied to other granular soils. The similarity of the value of $(\varepsilon_s^p)_{cv}$ for the soil tested by Rowe and the soil tested in this study seem to suggest that for the post-peak softening behaviour of the sand may not be sensitive to the value of $(\varepsilon_s^p)_{cv}$.

Wan and Guo (1998) presented a model for sand in which they used a modified version of Rowe's stress-dilatancy theory as a flow rule. They modified the stress-dilatancy theory by making it dependent on a state parameter related to the current critical voids ratio. Wan and Guo (1998) claimed that the modification to the flow rule was necessary in order to provide a realistic stress-dilatancy response in *R*-*D* space.

Wan and Guo however failed to recognize the fact that in general the Rowe friction angle, ϕ'_f, varies between ϕ'_μ and ϕ'_{cv} during shearing of the material and is not a constant as assumed by them. This results from the fact that sliding of particles occurs throughout deformation at a number of directions simultaneously, which deviates from the mean direction. More energy is therefore absorbed than for the case where all particles slide in the mean direction (Rowe, 1971a). The deviation of the sliding direction of the particles from the mean sliding direction manifests itself in a friction angle, ϕ'_f, greater than ϕ'_μ. During the shearing process, the value of ϕ'_f changes between ϕ'_μ and ϕ'_{cv}, where the deviation of the particle sliding direction from the mean is a maximum. It has been stated earlier that the largest part of the hardening in the

yield behaviour of the material results from the increase in the dilatancy behaviour of the material. The increase in the Rowe friction angle constitutes another small portion of the hardening behaviour of the material. This is illustrated in Figure C.4. It is interesting to note that the material exhibits a work softening behaviour after the peak strength has been reached, in spite of the fact that the ϕ'_f component continues to increase until the constant volume state is reached.

This is also illustrated by the relationships presented in Figure C.5. The maximum dilation rate is reached at point *a*. The material undergo a further strength increase due to the increase in ϕ'_f while the dilation rate decrease slightly. This is shown by the stress path *a*-*b* in Figure C.5. Non-uniform deformation in conventional triaxial testing often masks the distinction between point *a* and *b* in the test results.

The change in the ϕ'_f between ϕ'_μ and ϕ'_{cv} can be modelled as a work hardening process using the following equation:

$$\phi'_f = \left(\phi'_{cv} - \phi'_\mu\right) \cdot \left(1 - e^{-b \cdot \varepsilon_s^p}\right) + \phi'_\mu \qquad \text{(C.10)}$$

Where:

b = a parameter governing the rate of change of Rowe's friction angle between the two limiting angles.

This equation is equivalent to Equation (4.22) presented in Section 4.3.3 for ϕ'_f at peak, and the *b* parameter is the same.

The model parameters to adequately model the pre-peak and early stages of post-peak strain softening can be obtained from conventional triaxial tests. With conventional triaxial testing, reliable post-peak data is seldom available as strain localization just after the peak dilation causes a non-uniform deformation and shear band failure. It is, however, seldom necessary to accurately model the post-peak behaviour of the material.

With the equations presented in this section the mobilized dilation and friction angles can be obtained as a function of the plastic shear strain. The model can therefore easily be implemented into analytical calculation procedures and numerical analysis codes.

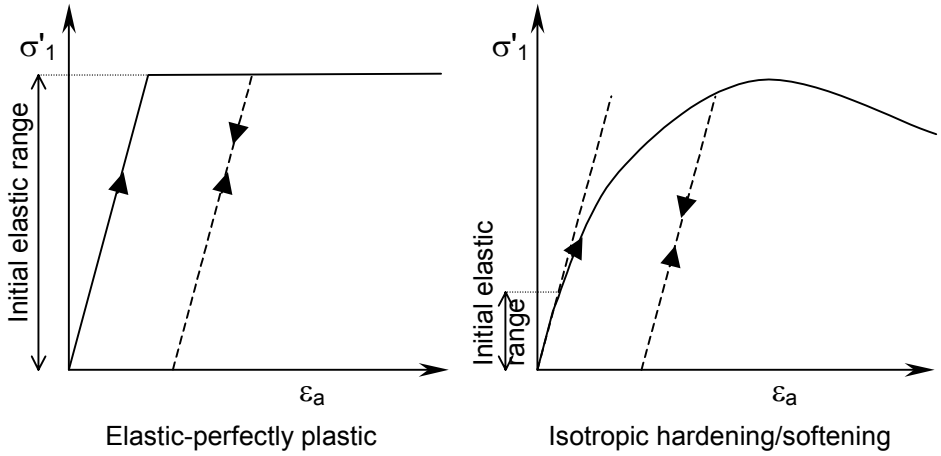

Figure C.1 *Diagrammatic illustration of the difference between elastic-perfectly plastic and elastic isotropic hardening/softening models.*

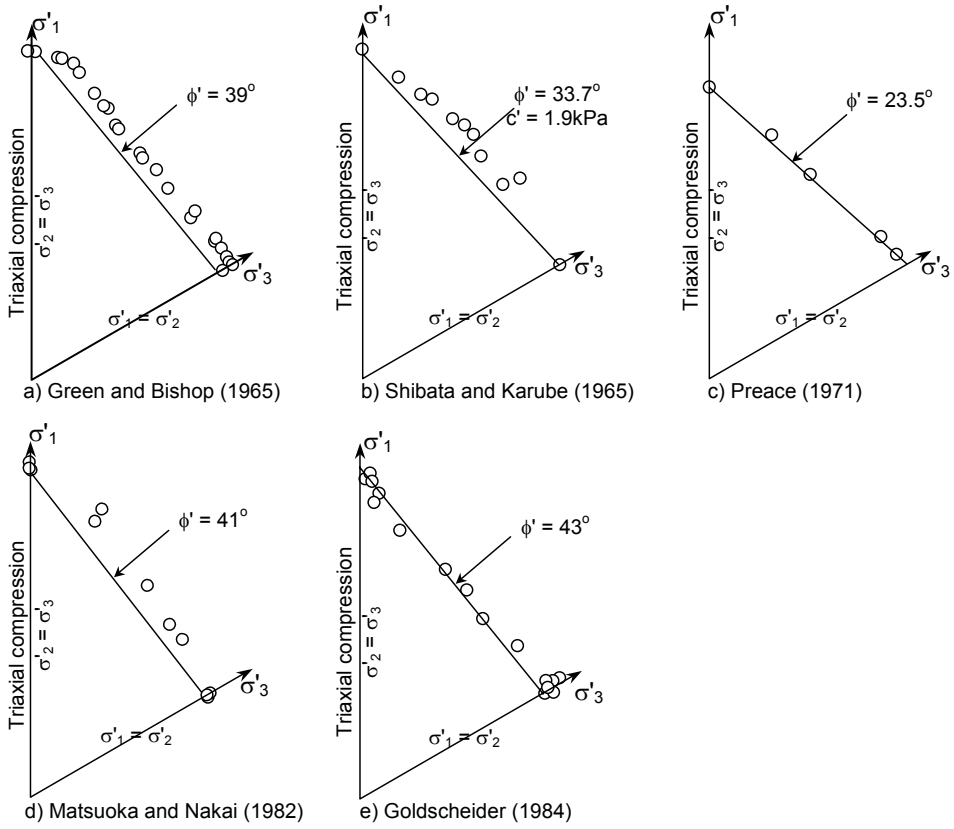

Figure C.2 *Comparison between measured and yield surfaces and the Mohr-Coulomb yield surface on the deviatoric stress plane for data presented in literature.*

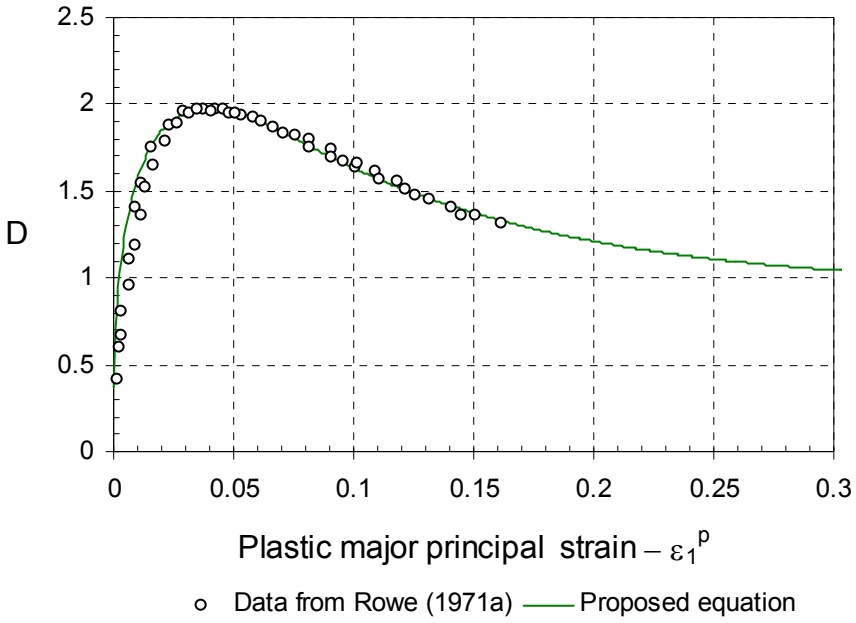

Figure C.3 *Comparison between the proposed equation and data presented by Rowe (1971a) for test on dense sand.*

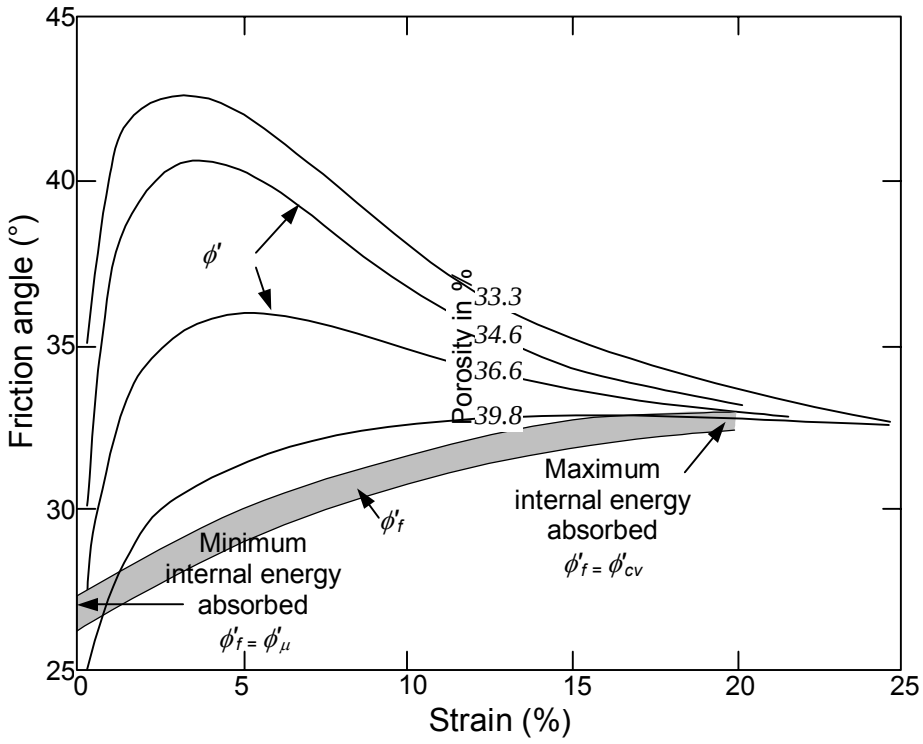

Figure C.4 *The change in ϕ'_f with plastic shear strain (Rowe, 1963).*

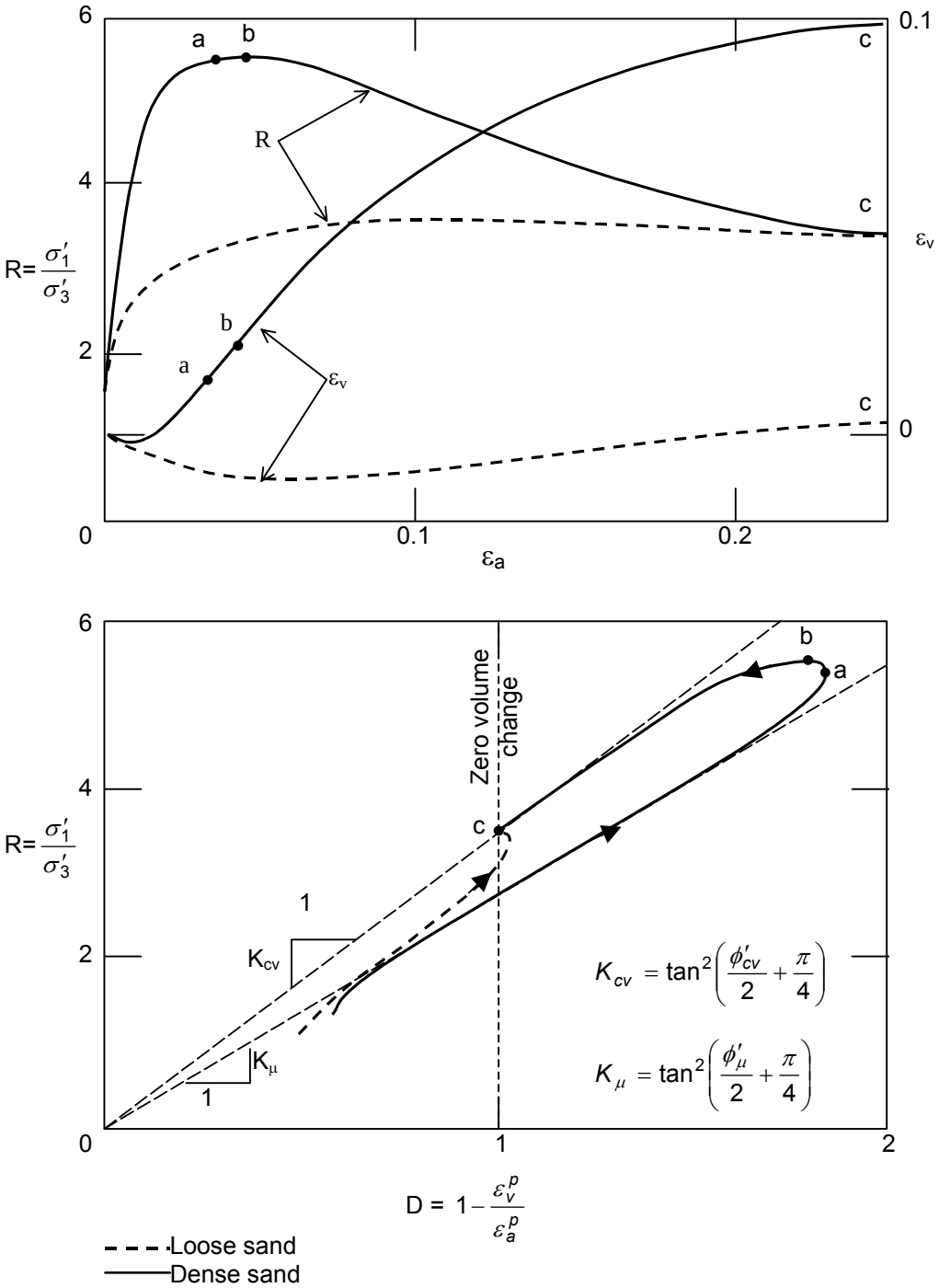

Figure C.5 *Typical results of triaxial tests on loose and dense sands shown in* R-D *space (Based on Horn, 1965).*

Appendix D

Formulation of mathematical models for the membrane behaviour

D.1 Introduction

The lack of a simple mathematical model to describe the stress-strain curves of geomembranes was recognised by both Giroud (1994) and Merry and Bray (1997).

The work of Giroud (1994) focussed on providing a simple and accurate function for the stress-strain curve between the origin and the yield peak in a uniaxial tensile test. All his tests were performed according to ASTM D-638 (1994) at a nominal strain rate of 100%/min. He showed that, under these conditions, the stress-strain curve of the geomembrane could satisfactorily be approximated by an *n*-order polynomial of which the parameters can easily be obtained from the uniaxial test results.

Merry and Bray (1997), on the other hand, were interested in the stress-strain behaviour of HDPE geomembranes under bi-axial loading at different strain rates. They proposed the use of the following empirical equation of a hyperbolic form:

$$\sigma(\varepsilon) = \frac{\varepsilon}{\frac{\beta}{E_s} + \frac{R_f \cdot \varepsilon}{\sigma_{max}}} \qquad \text{(D.1)}$$

Where:

$\sigma(\varepsilon)$ = the strain rate dependent stress,

ε = the strain,

E_s = the secant modulus at a particular strain as a function of strain rate,

β = the ratio of the secant modulus, E_s, to the initial

modulus,

R_f = the ratio of the maximum stress to a fictitious ultimate stress that is higher than the maximum stress,

σ_{max} = the maximum stress as a function of the strain rate.

The study by Merry and Bray included the use of hyperbolic tangent functions (after Prager) and the *n*-order polynomial functions (after Giroud, 1994). The Prager model was found not to produce acceptable representation of the strain-rate-dependent response of the HDPE geomembranes. Merry (1995) suggested modification to the variable *n*-order polynomial approach of Giroud (1994) and states that it compares favourably to the suggested hyperbolic model. The hyperbolic model, however, is favoured as it is more efficient in terms of the number of parameters needed.

D.2 A hyperbolic model for uniaxial membrane loading

Equation (D.1) can be used to describe the stress-strain behaviour of the geomembrane up to the transition point defined in Section 4.5.2. For this purpose σ_{max} can be substituted by the transition stress, σ_t. Using the secant modulus at the transition point, E_{st}, Equation (D.1) can be written as:

$$\sigma(\varepsilon) = \frac{\varepsilon}{\frac{\beta}{E_{st}} + \frac{R_f \cdot \varepsilon}{\sigma_t}} \tag{D.2}$$

Evaluating Equation (D.2) at the transition point, yields the following relationship:

$$R_f + \beta = 1 \tag{D.3}$$

This reduces Equation (D.2) to:

$$\sigma(\varepsilon) = \frac{\varepsilon}{\beta \cdot \varepsilon_t + (1-\beta) \cdot \varepsilon} \cdot \sigma_t \tag{D.4}$$

Where

σ_t = the transition stress and,

ε_t = the strain at the transition point,

β = the ratio of the secant modulus at the transition point, E_{st}, to the initial modulus.

In Section (4.5.2) it was shown that the relationship between the transition stress and the logarithm of the strain rate take the form of an "S"-curve. This part of the plastic behaviour can be modelled with Equation (D.5):

$$\sigma_t(\dot{\varepsilon}) = \frac{\sigma_{tmax} - \sigma_{tmin}}{1 + e^{-d_\sigma \cdot \ln(\dot{\varepsilon}) - e_\sigma}} + \sigma_{tmin} \qquad \text{(D.5)}$$

Where:

d_σ and e_σ = the parameters obtained from fitting the equation to the data,

σ_{tmax} and σ_{tmin} = the maximum and minimum asymptote value of the transition stress,

$\dot{\varepsilon}$ = the strain rate.

Generally, however, the geotechnical engineer would only be interested in the material behaviour at low strain rates. For this purpose the change in the transition stress with a change in the strain rates at low strain rates may be more easily approximated by another relationship of the following form:

$$\sigma_t(\dot{\varepsilon}) = \sigma_{tmin} + a_\sigma \cdot \log(\dot{\varepsilon})^{b_\sigma} \qquad \text{(D.6)}$$

Where:

a_σ and b_σ = the parameters obtained from fitting the equation to the data,

σ_{tmin} = the minimum asymptote value of the transition stress,

$\dot{\varepsilon}$ = the strain rate.

The β parameter can be obtained by fitting Equation (D.4) to the section of the data before the transition point. The values of β for the tested membranes are shown against the strain rate in Figure D.1. The β parameter is also dependent on the strain rate. Due to the scatter in the results the relationship between β and the strain rate is not clearly distinguishable. It would be reasonable, however, to expect that the value of β, like σ_t, would also approach asymptotic values at very low and very high strain rates. An "S"-curve similar to Equation (D.5) was used to approximate the data:

$$\beta(\dot{\varepsilon}) = \frac{\beta_{max} - \beta_{min}}{1 + e^{-d_\beta \cdot \ln(\dot{\varepsilon}) - e_\beta}} + \beta_{min} \qquad \text{(D.7)}$$

Where:

d_β and e_β = parameters obtained from fitting the

equation to the data,

β_{max} and β_{min} = the maximum and minimum asymptote value of β,

$\dot{\varepsilon}$ = the strain rate.

It should be noted that the accuracy of the stress-strain curves are not sensitive to the value of β (Cf. Figure 4.41). As a result the accuracy of β is therefore of less importance to the design engineer. For most applications, a constant value could be assumed for β without significant error.

The stress-strain curve shown in Figure 4.37 is essentially linear after the transition point and can be approximated with a line. Assuming a smooth transition between the hyperbolic and linear parts of the stress-strain curve, the gradient of the linear section of the curve should equal the gradient of the hyperbolic section of the curve at the transition point. The gradient is:

$$\frac{d}{d\varepsilon}\sigma(\varepsilon_t) = \frac{\sigma_t}{\varepsilon_t} \cdot \beta = E_{st} \cdot \beta \tag{D.8}$$

Where:

E_{st} = the secant modulus at the transition point.

Combining all the components of the membrane behaviour discussed above, the following mathematical model consisting of a form function ($B(\dot{\varepsilon})$) and a magnitude function ($\sigma_t(\dot{\varepsilon})$) is obtained.

$$\sigma(\varepsilon, \dot{\varepsilon}) = B(\varepsilon, \dot{\varepsilon}) \cdot \sigma_t(\dot{\varepsilon}) \tag{D.9}$$

Where:

$$B(\varepsilon, \dot{\varepsilon}) = \begin{cases} \dfrac{\varepsilon}{\beta(\dot{\varepsilon}) \cdot \varepsilon_t + (1 - \beta(\dot{\varepsilon})) \cdot \varepsilon} & \text{if } \varepsilon \le \varepsilon_t \\ 1 + \dfrac{\beta(\dot{\varepsilon})}{\varepsilon_t} \cdot (\varepsilon - \varepsilon_t) & \text{if } \varepsilon > \varepsilon_t \end{cases} \tag{D.10}$$

With

$\dot{\varepsilon}$ = the strain rate,

$\beta(\dot{\varepsilon})$ and $\sigma_t(\dot{\varepsilon})$ = the strain rate dependent functions presented earlier.

The parameters for the above mentioned model obtained from the data are presented in Table D.1.

Table D.1 Parameters for the hyperbolic model obtained from data.

β				σ_t				ε_t
β_{max}	β_{min}	d_β	e_β	$\sigma_{t\,max}$	$\sigma_{t\,min}$	d_σ	e_σ	
0.304	0.187	0.6	0.35	15	7.45	0.737	-0.345	0.16

Figure D.2 shows the original data with the model curve using the parameters in Table D.1. The assumption that the gradient of the linear section of the curve is equal to the gradient of the hyperbolic section of the curve at the transition point seems to be adequate. It would therefore be possible to obtain an estimate of β from the gradient of the linear section of the curve, that is:

$$\beta = a \cdot \frac{\varepsilon_t}{\sigma_t} = \frac{a}{E_{st}} \tag{D.11}$$

Where:

a = the gradient of the linear section of the curve in stress units,

E_{st} = the secant modulus at the transition point.

Figure D.3 shows the comparison between the values of β obtained through a curve fitting procedure through the hyperbolic section of the curve and the values obtained from the gradient of the linear section.

The initial stiffness of a geomembrane is often of interest to the engineer but is difficult to measure (Giroud, 1994). From the derivative of Equation (D.4), it can be shown that the ratio of the tangent modulus at zero strain to the secant modulus at the transition point is equal to the inverse of β:

$$\frac{E_{t0}}{E_{st}} = \frac{1}{\beta} \tag{D.12}$$

The ratio of tangent modulus at zero strain to the secant modulus at the transition point for the tested geomembrane vary from 3.5 at 0.04%/min to 4.9 at 100%/min. A value of about 4, for the ratio of the tangent modulus at zero strain to the secant modulus at the "yield"-point has been suggested by Giroud (1994).

The hyperbolic model, although adequate for describing the geomembrane behaviour, has two important drawbacks: the necessity for choosing a transition point and the fact that the model consists of two separate equations for the

regions before and after the transition point. Another model that does not suffer these drawbacks is presented in the following section.

D.3 An exponential model for uniaxial membrane loading

The following empirical equation (Equation (D.13)) can also be used to model the geomembrane behaviour under uniaxial loading conditions:

$$\sigma(\varepsilon) = (a \cdot \varepsilon + c) \cdot (1 - e^{-b \cdot \varepsilon}) \tag{D.13}$$

Where

a, b and c = strain rate dependent parameters that can be obtained from simple laboratory tests,

ε = the strain.

A non-linear "curve-fitting" technique was applied to the available data to obtain the parameters for the test performed at different strain rates. Statistical tests on the calculated b parameter indicated that it could be assumed to be independent of strain rate. The relationship of a and c with strain rate are shown in Figure D.4 and Figure D.5.

The c parameter is similar to the transition stress and seems to behave similar to changes in strain rate and can also be approximated with an "S"-curve of the form shown in Equation (D.14):

$$c(\dot{\varepsilon}) = \frac{c_{max} - c_{min}}{1 + e^{-d_c \cdot \ln(\dot{\varepsilon}) - e_c}} + c_{min} \tag{D.14}$$

Where:

d_c and e_c = parameters obtained from fitting the equation to the data,

c_{max} and c_{min} = the maximum and minimum asymptote value of the c parameter,

$\dot{\varepsilon}$ = the strain rate.

As geotechnical engineers are more interested in the behaviour of the geomembrane at lower strain rates, the value of c may be more easily approximated by the following equation:

$$c(\dot{\varepsilon}) = c_{min} + a_c \cdot \log(\dot{\varepsilon})^{b_c} \tag{D.15}$$

Where:

a_c and b_c = parameters obtained from fitting the equation to the data,

c_{min} = the minimum asymptote value of the c parameter,

$\dot{\varepsilon}$ = the strain rate.

As with β it is reasonable to expect a to approach asymptotic values at very low and very high strain rates. The line shown in (Figure D.4) was obtained by fitting the following "S"-curve to the data:

$$a(\dot{\varepsilon}) = \frac{a_{max} - a_{min}}{1 + e^{-d_a \cdot \ln(\dot{\varepsilon}) - e_a}} + a_{min} \qquad \text{(D.16)}$$

Where:

d_a and e_a = parameters obtained from fitting the equation to the data,

a_{max} and a_{min} = the maximum and minimum asymptote value of a,

$\dot{\varepsilon}$ = the strain rate.

As with β the accuracy of the stress-strain curves are not sensitive to the value of a and for most applications a constant value could be assumed for a without significant error.

The parameters obtained from the data are shown in Table D.2. Figure D.6 compares the exponential model and the original data, using the parameters from Table D.2. The exponential model compares favourably with the hyperbolic model.

Table D.2 Parameters for the exponential model obtained from data.

a				**c**				**b**
a_{max}	a_{min}	d_a	e_a	c_{max}	c_{min}	d_c	e_c	
17.54	14.12	1.931	1.172	12.45	4.79	0.651	-0.287	32.517

Figure D.7 illustrates the mathematical meaning of the parameters in the equation. It is possible to estimate the parameters from the data by obtaining the slope and intercept of the section of the curve after the transition point and the slope at zero strain. The b parameter can also be estimated from a and c

and an arbitrarily chosen point *k* located on the section of the experimentally obtained curve before the transition point by using the following equation derived from Equation (D.13).

$$b = -\ln\left(1 - \frac{\sigma_k}{a \cdot \varepsilon_k + c}\right) \cdot \frac{1}{\varepsilon_a} \tag{D.17}$$

Where:

a, b and c = parameters,

σ_k and ε_k = the measured stress and strain at an arbitrarily chosen point on the stress-strain curve before the transition point.

Figure D.8 compares the values of the model parameters obtained with non-linear curve fitting techniques and the simplified method described above. As would be expected, for the parameters *a* and *c*, a one to one relationship exists between the parameter values obtained with the two methods, albeit with a fair amount of scatter. For most practical applications, the simplified method for obtaining the model parameters will suffice. The value of *b* obtained from Equation (D.17) is less accurate as only a single measurement is used. The obtained value of *b* varies with different chosen *k*-points. A value of 30.6 ± 2.5 was obtained when point, *k*, was chosen at a strain of 0.05 and a value of 32.2 ± 6.7 was obtained at a strain of 0.03. The value for *b* obtained through the non-linear curve fitting technique was 32.52 ± 1.3.

From the derivative of Equation (D.13) the tangent modulus at zero strain can be estimated, that is:

$$E_{t0} = b \cdot c \tag{D.18}$$

The values of the tangent modulus at zero strain estimated in this manner vary from about 3.5 times the secant modulus at the transition point at a strain rate of 0.04%/min to about 4.25 times the secant modulus at the transition point at a strain rate of 100%/min.

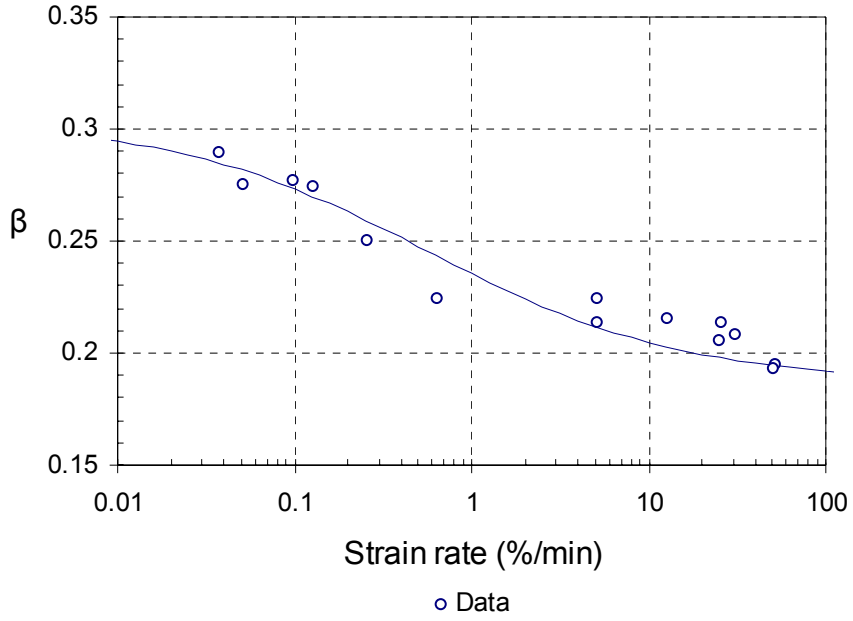

Figure D.1 *The relationship between the β parameter and strain rate.*

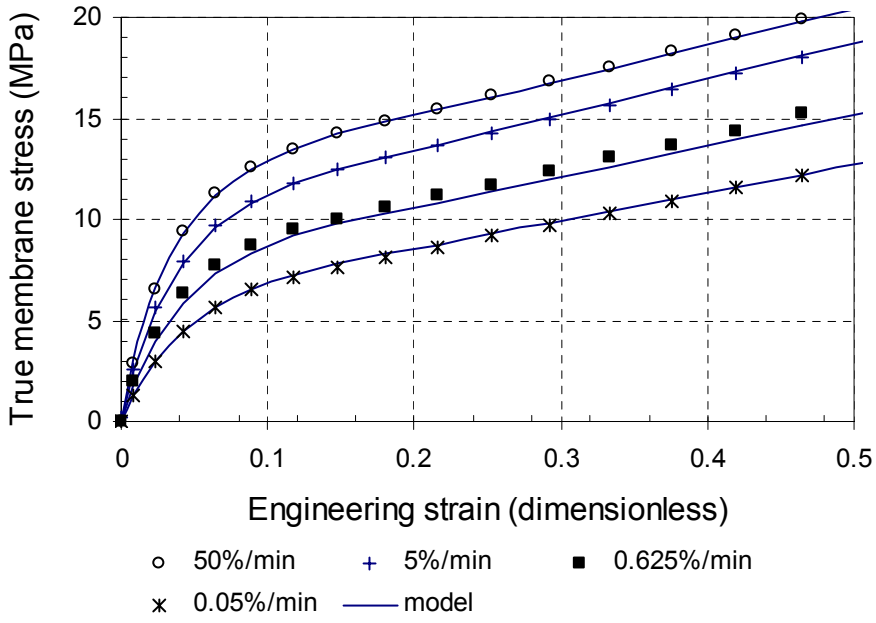

Figure D.2 *Comparison between the hyperbolic model and the original data.*

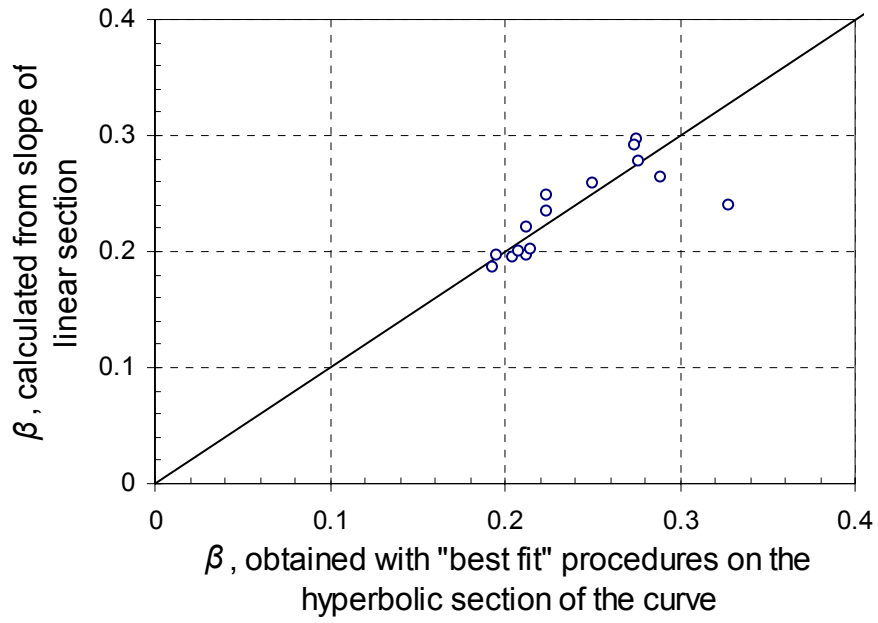

Figure D.3 *Comparison between the β parameter obtained from different parts of the stress-strain curve.*

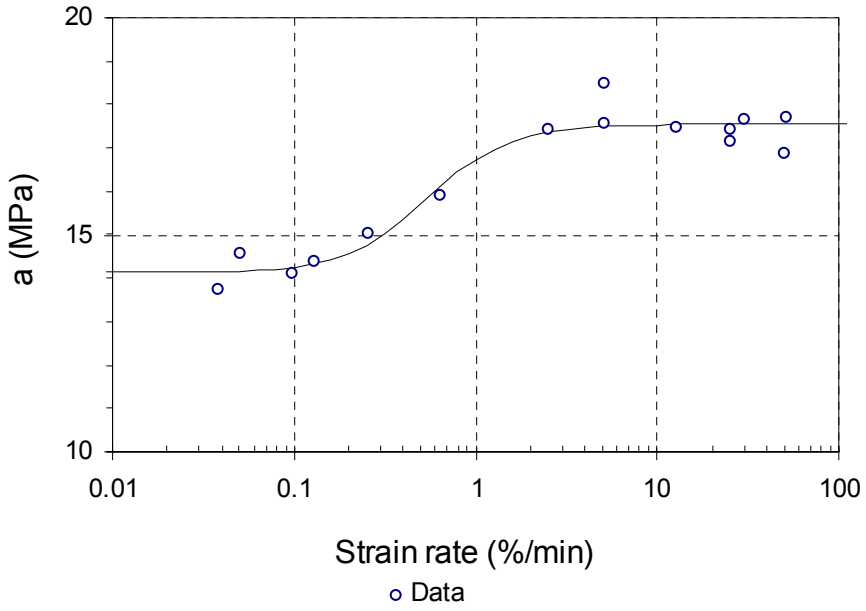

Figure D.4 *The relationship between the parameter, a, and strain rate.*

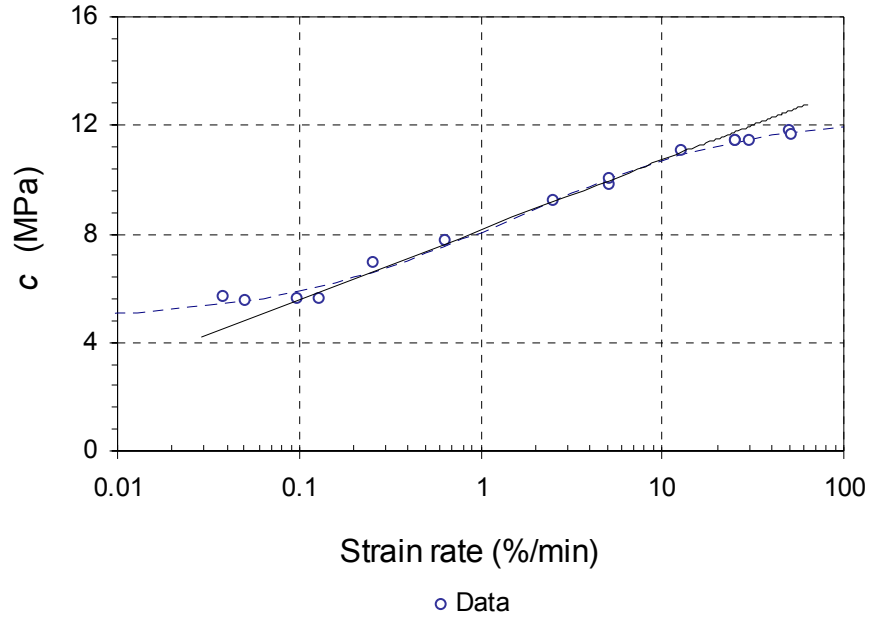

Figure D.5 *The relationship between* c *and strain rate.*

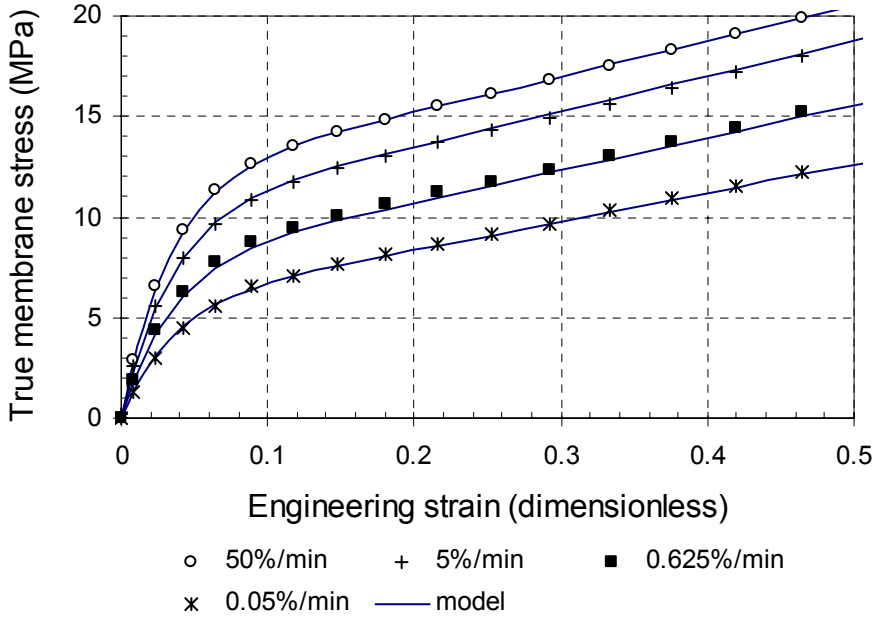

Figure D.6 *Comparison between the exponential model and the original data.*

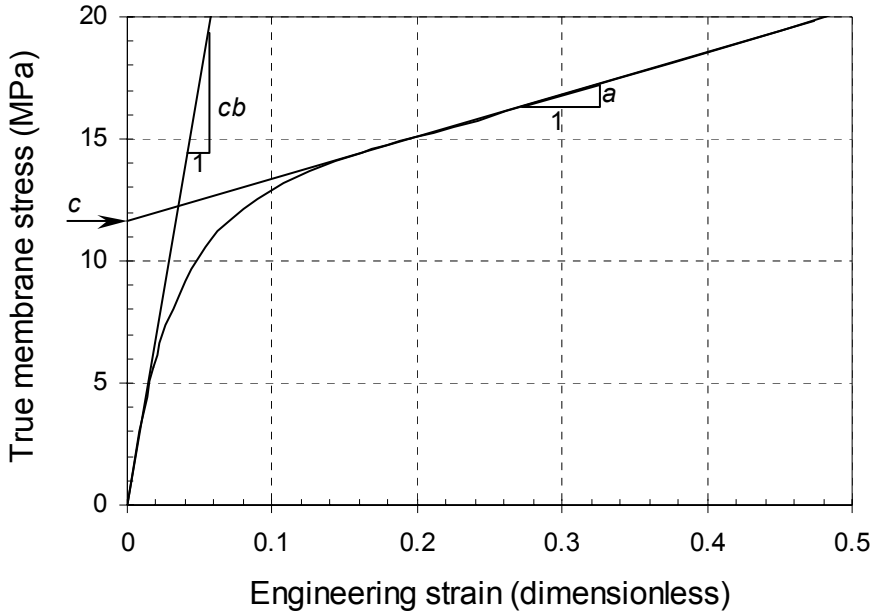

Figure D.7 *Illustration of the mathematical meaning of the parameters of the exponential model.*

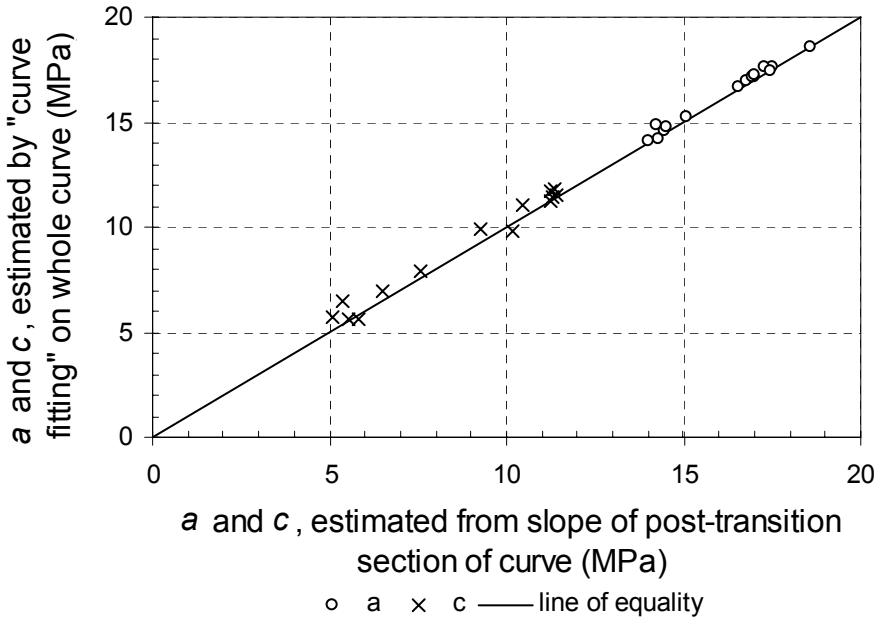

Figure D.8 *Comparison between the values of* a *and* c *obtained by different methods.*

Appendix E

The mean shearing direction of a soil element

E.1 The mean shearing direction after the development of a shear band

When a rupture surface (shear band) develops in the soil, the direction of the shear band, θ, will be equal to χ. Consider therefore, the angle at which a shear band will develop in a granular material.

Zitóuni (1988) stated that the direction of the dominant shear band could be arrived at, either by considering the stress state, or the state of deformation. The approach based on the consideration of the stress state, assumes that the shear band will form along the plane of maximum stress obliquity and leads to the following equation for θ:

$$\theta = \frac{\phi'}{2} + 45° \qquad \text{(E.1)}$$

Where:

ϕ' = the Mohr-Coulomb friction angle.

Equation (E.1) has traditionally been viewed as the angle between the minor compressive stress and the shear band or rupture surface.

Considering the state of deformation, Roscoe (1970) suggested that rupture surfaces forms along zero extension lines which leads to the following relationship for θ:

$$\theta = \frac{\psi}{2} + 45° \qquad \text{(E.2)}$$

Where:

ψ = the dilation angle.

It has been demonstrated experimentally and theoretically (Arthur, et al., 1977a; Arthur, et al., 1977b, Vardoulakis 1980) that both the "Coulomb" and "Roscoe" solutions are possible. Both Arthur et al. (1977b) and Vardoulakis (1980) concluded that θ would fall between the "Coulomb" and "Roscoe" solutions and suggested the following equation for θ:

$$\theta = \frac{\phi'_{mob} + \psi_{mob}}{4} + 45° \qquad \text{(E.3)}$$

Where:

ϕ'_{mob} = the mobilized Mohr-Coulomb friction angle at the strain where the shear band develops,

ψ_{mob} = the mobilized dilation angle at the strain where the shear band develops.

Vermeer (1982) has shown that Equation (E.3) corresponds to the lowest bifurcation point in the stress-strain curve and suggests that, due to small imperfections in the soil samples, it is likely that such samples would bifurcate at the lowest bifurcation point. Saada et al. (1999) reported that the best correlation between the measured and calculated inclination angle of the shear band was obtained by using Equation (E.3) with the maximum dilation angle and the peak friction angle obtained from torsion tests.

Recently Lade (2003) presented a model for the analysis and prediction of shear banding in granular materials. He performed true triaxial tests with a *b*-value varying between 0 and 1. The *b*-value being defined as follows:

$$b = \frac{\sigma'_2 - \sigma'_3}{\sigma'_1 - \sigma'_3} \qquad \text{(E.4)}$$

Where:

$\sigma'_1, \sigma'_2, \sigma'_3$ = the major, minor and intermediate principal stress.

The *b*-value is 0 for triaxial compression tests, 1 for triaxial extension tests and approximately 0.23 for plane strain conditions. It is interesting to note that for dense Santa Monica Beach sand, the predictions made by the model proposed by Lade (2003) varies around the values predicted by Equation (E.3). The

value of θ, predicted by Lade's model increases monotonically form $b = 0$ to $b = 1$ and is equal to the values given by Equation (E.3) at $b \approx 0.5$. The data presented by Lade, however, seems to suggest that θ is equal to the value predicted by Equation (E.3), increasing to a asymptote value predicted by Equation (E.1) as the *b*-value increases to 1 (Figure E.1).

Although there is some disagreement between researchers of the bifurcation phenomenon, from the above-mentioned literature, it seems that there is general consensus that the shear band inclination is bounded by the limits given by the "Coulomb" and "Roscoe" solutions (Equation (E.1) and (E.2)), and that Equation (E.3) provides a good estimation of the inclination of the shear band.

E.2 The mean shearing direction in a soil element before the development of a shear band

Rowe (1971a) describes the plastic deformation of granular material as interlocked groups of particles sliding instantaneous against each other before reforming into new groups. This mechanism is described by Arthur et al. (1977b) as a random distribution of local simple shears. As the strain in the soil increases the local zones of simple shear combine to form rupture surfaces with an inclination between the "Coulomb" and "Roscoe" solution. An inclination given by Equation (E.2) will result from a combination of simple shears at different locations, half of which are in a no-extension direction of the total strain increment (Equation (E.2)) while the other half are on a maximum stress obliquity plane (Equation (E.1)) (Arthur et al. 1977b). It is reasonable to believe that the random distribution of local simple shears in the two directions would be the same before and after shear bands develop. The author therefore, suggests that the mean shearing direction of elements of granular soil in a sample, χ, could be estimated by Equation (E.2), assuming χ to be equal to θ throughout the strain hardening regime:

$$\beta = \chi = \frac{\phi'_{mob} + \psi_{mob}}{4} + 45° \qquad \text{(E.5)}$$

Where:

ϕ'_{mob} = the mobilized Mohr-Coulomb friction angle,

ψ_{mob} = the mobilized dilation angle.

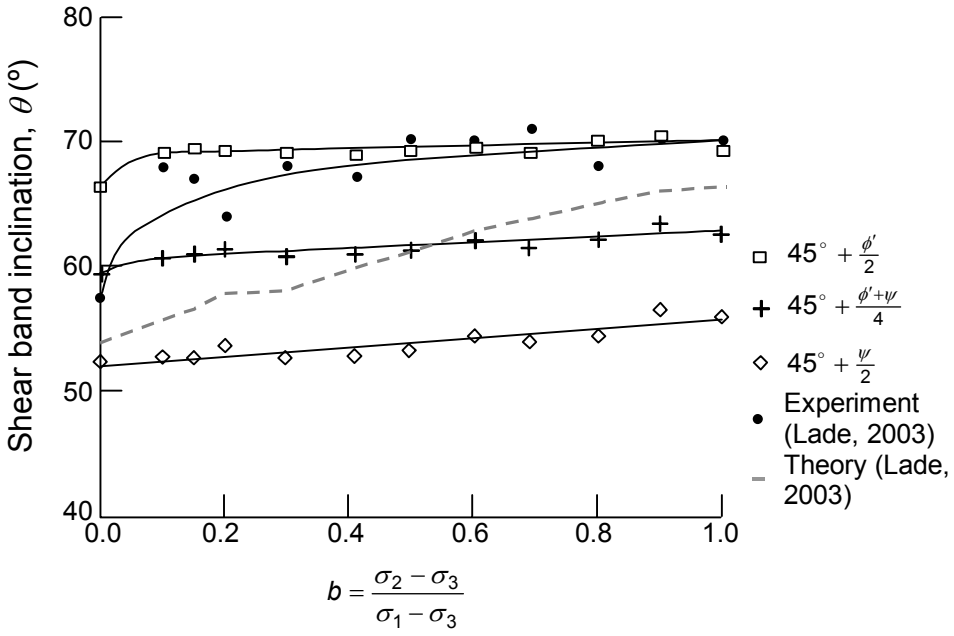

Figure E.1 *Experimental shear band inclinations for dense Santa Monica Beach sand (based on Lade 2003).*